JOURNAL OF THERMOPHYSICS AND HEAT TRANSFER
Vol. 11, No. 1, January–March 1997

Mixed Convection in the Laminar Flow of Viscoelastic Liquids Through Rectangular Ducts

Mônica F. Naccache* and Paulo R. Souza Mendes*
Pontifícia Universidade Católica, Rio de Janeiro RJ 22453-900, Brazil

Flow patterns and heat transfer coefficients are obtained for the fully developed flow of viscoelastic liquid flowing laminarly inside ducts of rectangular cross sections. The effect of natural convection is analyzed. The results are obtained by integrating the conservation equations together with the Criminale–Ericksen–Filbey constitutive model, via a control-volume technique. Wide ranges of the relevant parameters are investigated. Different flow regimes are observed, depending upon the relative importance of viscoelastic and buoyancy-driven forces. These changes in flow regime are responsible for dramatic changes in the heat transfer behavior, which have been previously observed experimentally, as reported in the literature.

Nomenclature

a = parameter of the Carreau–Yasuda equation, Eq. (15)
B = duct width, m
c = specific heat, J/kg K
D_h = duct hydraulic diameter, m
$\hat{\boldsymbol{e}}_x$, $\hat{\boldsymbol{e}}_y$, $\hat{\boldsymbol{e}}_z$ = unit vectors in the x, y, and z directions, respectively, Fig. 1
f = friction factor, $\equiv [2(\partial p/\partial z)D_h]/(\rho \bar{w}^2)$
g = magnitude of the acceleration caused by gravity, m/s^2
$\mathbf{g}$ = acceleration caused by gravity, $-g\hat{\mathbf{e}}_y$, m/s^2
H = duct height, m
k = thermal conductivity, W/mK
n = power-law exponent of the Carreau–Yasuda equation, Eq. (15)
P = dimensionless pressure
p = pressure, Pa
q_w = wall heat flux, W/m^2
$T(x, y, z)$ = temperature field, °C
$T_m(z)$ = bulk temperature, °C
$T_{w,b}(x, z)$ = wall temperature distribution at bottom wall, °C
$\bar{T}_{w,b}(z)$ = mean wall temperature at bottom wall, °C
$T_{w,t}(x, z)$ = wall temperature distribution at top wall, °C
$\bar{T}_{w,t}(z)$ = mean wall temperature at top wall, °C
$\bar{T}_w(z)$ = characteristic wall temperature, °C
U, V, W = dimensionless velocity components
u = x component of velocity, m/s
v = y component of velocity, m/s
$\boldsymbol{v}$ = velocity vector field, m/s
X, Y, Z = dimensionless coordinates
x = horizontal crosswise coordinate, m
y = vertical coordinate, m
$\bar{W}$ = dimensionless mean axial velocity
We = Weissenberg number
w = z component of velocity (axial velocity), m/s
$\bar{w}$ = mean axial velocity, m/s
z = axial coordinate, m
α = duct aspect ratio, $\equiv B/H$
β = coefficient of thermal expansion, $\equiv [\partial\rho(p, T)/\partial T]/\rho$, K^{-1}
$\dot{\gamma}$ = deformation rate, $\equiv \sqrt{\frac{1}{2}\ \mathrm{tr}\ \dot{\boldsymbol{\gamma}}^2}$, s^{-1}
$\dot{\boldsymbol{\gamma}}$ = rate-of-deformation tensor, s^{-1}
$\dot{\gamma}^*$ = dimensionless deformation rate, $\equiv \dot{\gamma}/\dot{\gamma}_c$
$\dot{\gamma}_c$ = characteristic deformation rate, s^{-1}
$\boldsymbol{\gamma}_{[2]}$ = second rate-of-deformation tensor, s^{-2}
$\Delta\psi$ = stream function difference, $\equiv \psi_{\max} - \psi_{\min}$, kg/m s
η = viscosity function, kg/m s
η^* = dimensionless viscosity function
η_c = characteristic viscosity, kg/m s
η_0 = zero-shear rate viscosity, kg/m s
η_0^* = dimensionless zero-shear rate viscosity
η_∞ = infinite-shear rate viscosity, kg/m s
η_∞^* = dimensionless infinite-shear rate viscosity
$\bar{\theta}_{w,b}$ = dimensionless mean wall temperature at bottom wall
$\theta_{w,b}(X)$ = dimensionless wall temperature distribution at bottom wall
$\bar{\theta}_{w,t}$ = dimensionless mean wall temperature at top wall
$\theta_{w,t}(X)$ = dimensionless wall temperature distribution at top wall
$\theta(X, Y)$ = dimensionless temperature
λ = characteristic time of fluid, s
$\boldsymbol{\tau}$ = extra-stress tensor, Pa
$\boldsymbol{\tau}^P$ = polymeric part of τ, Pa
$\boldsymbol{\tau}^{P*}$ = dimensionless τ^P
Ψ_1 = first normal stress coefficient, Pa s^2
Ψ_2 = second normal stress coefficient, Pa s^2
Ψ_1^* = dimensionless first normal stress coefficient
Ψ_2^* = dimensionless second normal stress coefficient
ψ = stream function, defined by $\partial\psi/\partial x \equiv -\rho v$, $\partial\psi/\partial y \equiv \rho u$, $\partial\psi/\partial z \equiv 0$, kg/m s
$\psi_{\max}$ = maximum value of the stream function, kg/m s
$\psi_{\min}$ = minimum value of the stream function, kg/m s

Introduction

NON-NEWTONIAN liquids are present in a wide variety of industrial processes. Paints, several foods, plastics, petroleum, and most cosmetics are a few examples of non-Newtonian liquids. Any process that involves the flow of one of these liquids must be designed considering the rheological behavior of the material, which is usually rather complex. Therefore, the modern process engineer must be acquainted with the field of rheology.

Received Jan. 19, 1996; revision received Aug. 21, 1996; accepted for publication Aug. 30, 1996.

*Professor, Department of Mechanical Engineering.

There are several aspects that differ the flow of a viscoelastic liquid from the flow of a Newtonian liquid inside ducts.[1] Shear thinning effects decrease the shear stress in the neighborhood of the duct walls, decreasing pressure loss and increasing heat transfer rates. Secondly, the fully developed flow of a viscoelastic liquid in ducts of a noncircular cross section is generally not purely axial as in the Newtonian case.[2–4] Although the secondary flows that appear in the cross-sectional plane typically do not affect pressure losses,[5] they may triple or quadruple the heat transfer coefficients.[6,7] Nevertheless, these secondary flows caused by elasticity have often been disregarded.[8–11]

Because phenomena involving viscoelastic liquids are normally difficult to predict, most analyses typically assume isothermal conditions. However, this assumption is usually far from the reality found in industrial process flows. Most viscoelastic liquids are quite viscous, with viscosities typically ranging from 1 to 10^5 Pa s (Bird et al.[12]). Heating caused by viscous dissipation of mechanical energy is therefore present in many situations.[13] For low-viscosity liquids, viscous heating is generally unimportant, but, for analyses of cooling or heating processes, the usual assumption of isothermal conditions is obviously unsuitable.

The flow of non-Newtonian liquids through ducts has been studied by a number of authors. Townsend et al.[14] studied numerically and experimentally the flow through square ducts of a viscoelastic liquid, and observed the existence of secondary flows in the cross-sectional plane. These secondary flows are in the form of eight vortices arranged symmetrically. Gervang and Larsen[15] presented numerical results for other aspect ratios, and also observed the presence of vortices. They noted that, as the aspect ratio is increased, the vortices change in shape, strength, and size.

The heat transfer problem has also been investigated for this flow. For purely viscous non-Newtonian fluids, Chandrupatla and Sastri[16] and Gringrich et al.[11] have shown that for shear thinning fluids heat transfer is more intense than for Newtonian fluids. For shear thickening fluids, the opposite trend is observed.

For viscoelastic fluids, heat transfer rates are typically larger than for Newtonian fluids. Mena et al.[5] investigated flows of polymeric solutions in triangular and rectangular ducts, whereas Naccache and Souza Mendes[7] analyzed numerically fully developed flows through rectangular ducts of different aspect ratios. Gao and Hartnett[17] studied this problem with the aid of the Reiner–Rivlin model, which is capable of predicting nonzero second-normal stress coefficients. This model, however, predicts a null first-normal stress coefficient, which is shown by Naccache and Souza Mendes[7] to have significant effects in the secondary flow strength, and hence, in heat transfer. Hartnett and Kostic[6] studied experimentally the thermal entrance region of rectangular ducts, and compared results for viscoelastic and Newtonian fluids. Their results suggested that secondary flows are responsible for the heat transfer enhancement observed. However, no flow visualization results have been reported. Dunwoody and Hamill[18] analyzed both the dynamic and the thermal problems numerically, using as constitutive equation the third-order fluid model. Hartnett[1] and Kostic[19] offer comprehensive surveys on the subject.

Some polymeric solutions of engineering interest (found, e.g., in the food industry and in coating applications) have viscosities as low as the one of water ($\sim 10^{-3}$ Pa s). In flows of low-viscosity liquids, buoyancy forces may play an important role, interacting with the viscoelastic forces to change flow patterns and affect heat transfer rates.

For a Newtonian fluid, Maughan and Incropera[20] present results for mixed convection in finned parallel plate channels, which, in the case of fin length equal to the plate spacing, pertain to rectangular channels. They showed that the presence of natural convection causes Nu increases because of the secondary flows that appear.

This article analyzes the laminar flow of a viscoelastic liquid through a duct of rectangular cross section, in the presence of natural convection. More details are reported by Naccache.[21] As far as the authors know, natural convection effects have not been considered by any of the previously published articles that analyze this physical situation.

Analysis

The problem under analysis is described with the aid of Fig. 1.

A viscoelastic fluid flows through a duct of rectangular cross section, with aspect ratio $\alpha \equiv B/H$. The top and bottom walls are uniformly and symmetrically heated (q_w = constant at both walls). The side (vertical) walls are adiabatic.

The flow is assumed to be laminar and steady, and the fluid compressibility is neglected. The Boussinesq approximation is assumed to be applicable, and otherwise the effect of temperature on the thermophysical properties is neglected.

Velocity and temperature fields are obtained by integrating numerically the conservation equations in conjunction with an appropriate constitutive equation that describes the non-Newtonian mechanical behavior of the flowing liquid.

Conservation Equations

The mass and momentum equations for this flow can be written as

$$\operatorname{div} \boldsymbol{v} = 0 \tag{1}$$

$$\rho \operatorname{div}(\boldsymbol{v}\boldsymbol{v}) = -\operatorname{grad} p + \operatorname{div} \boldsymbol{\tau} + \rho \mathbf{g}[1 - \beta(T - T_m)] \tag{2}$$

$\boldsymbol{\tau}$ is the part of the stress tensor that vanishes when there is no motion other than rigid-body translation and rotation, and is a function of the flow kinematics. For viscoelastic fluid behavior, it is often convenient to decompose $\boldsymbol{\tau}$ into two terms, namely, a Newtonian-like term, and $\boldsymbol{\tau}^P$. The latter depends on the constitutive equation chosen:

$$\boldsymbol{\tau} = \eta(\dot{\gamma})\dot{\boldsymbol{\gamma}} + \boldsymbol{\tau}^P \tag{3}$$

In Eq. (3), $\dot{\boldsymbol{\gamma}} = \operatorname{grad} \boldsymbol{v} + (\operatorname{grad} \boldsymbol{v})^T$ is the rate-of-deformation tensor. $\dot{\gamma}$ is defined as $\dot{\gamma} \equiv \sqrt{\frac{1}{2} \operatorname{tr} \dot{\boldsymbol{\gamma}}^2}$.

The quantity $T_m(z)$, appearing in the buoyancy term of the momentum equation, is the bulk temperature, defined by

$$T_m = \frac{1}{\bar{w}BH} \int_0^H \int_0^B wT \, dx \, dy \tag{4}$$

Because the temperature field appears in the buoyancy term of the momentum equation, Eqs. (1) and (2) must be solved

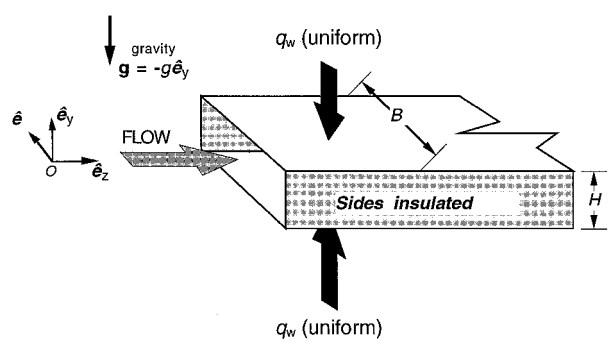

Fig. 1 Geometry and thermal boundary conditions.

in conjunction with the energy equation, which in the present case takes the form

$$\rho c \mathbf{v} \cdot \text{grad } T = \kappa \nabla^2 T \tag{5}$$

Before proceeding to a nondimensionalization of the governing equations, some characteristic quantities must be chosen. D_h, which is the characteristic length chosen in the present analysis, is given by $D_h = 2B/(1 + \alpha)$. The characteristic velocity is chosen to be $\bar{w}$. The quantity $\dot{\gamma}_c$ is a representative shear rate, defined as

$$\dot{\gamma}_c \equiv \frac{8\bar{w}}{D_h}\frac{3n+1}{4n} \tag{6}$$

Accordingly, the characteristic value of the viscosity function (to be defined later) is given by $\eta_c \equiv \eta(\dot{\gamma}_c)$.

Some dimensionless parameters and variables are now introduced:

$$X = x/D_h \qquad Y = y/D_h \qquad Z = z/D_h \qquad U = u/\bar{w}$$
$$V = v/\bar{w} \qquad W = w/\bar{w} \qquad \theta = (T - T_m)/(q_w D_h/k)$$
$$\boldsymbol{\tau}^{P*} = \boldsymbol{\tau}^P/\rho\bar{w}^2 \qquad P = (p + \rho g y)/\rho\bar{w}^2 \qquad \eta^* = \eta/\eta_c \tag{7}$$
$$Ra = \rho^2 c g \beta D_h^4 q_w/\eta_c \kappa^2 \qquad Pr = c\eta_c/\kappa$$
$$Re = \rho\bar{w}D_h/\eta_c \qquad \Psi_1^* = \Psi_1/\rho D_h^2 \qquad \Psi_2^* = -\Psi_2/\rho D_h^2$$

Using 1) the previous definitions, 2) the Cartesian coordinate system shown in Figs. 1 and 2, and 3) the fully developed flow assumption, the conservation equations take the following dimensionless form:

$$\frac{\partial U}{\partial X} + \frac{\partial V}{\partial Y} = 0 \tag{8}$$

$$U\frac{\partial U}{\partial X} + V\frac{\partial U}{\partial Y} = -\frac{\partial P}{\partial X} + \frac{1}{Re}\left[\frac{\partial}{\partial X}\left(2\eta^*\frac{\partial U}{\partial X}\right) + \frac{\partial}{\partial Y}\left(\eta^*\frac{\partial U}{\partial Y} + \eta^*\frac{\partial V}{\partial X}\right)\right] + \left(\frac{\partial \tau_{xx}^{P*}}{\partial X} + \frac{\partial \tau_{yx}^{P*}}{\partial Y}\right) \tag{9}$$

$$U\frac{\partial V}{\partial X} + V\frac{\partial V}{\partial Y} = -\frac{\partial P}{\partial Y} + \frac{1}{Re}\left[\frac{\partial}{\partial Y}\left(2\eta^*\frac{\partial V}{\partial Y}\right) + \frac{\partial}{\partial X}\left(\eta^*\frac{\partial V}{\partial X} + \eta^*\frac{\partial U}{\partial Y}\right)\right] + \left(\frac{\partial \tau_{xy}^{P*}}{\partial X} + \frac{\partial \tau_{yy}^{P*}}{\partial Y}\right) + \frac{Ra}{Re^2 Pr} \tag{10}$$

$$U\frac{\partial W}{\partial X} + V\frac{\partial W}{\partial Y} = -\frac{\partial P}{\partial Z} + \frac{1}{Re}\left[\frac{\partial}{\partial X}\left(\eta^*\frac{\partial W}{\partial X}\right) + \frac{\partial}{\partial Y}\left(\eta^*\frac{\partial W}{\partial Y}\right)\right] + \left(\frac{\partial \tau_{xz}^{P*}}{\partial X} + \frac{\partial \tau_{yz}^{P*}}{\partial Y}\right) \tag{11}$$

where τ_{ij}^{*P} is the ijth component of $\boldsymbol{\tau}^{*P}$.

The dimensionless energy equation is written as

$$U\frac{\partial \theta}{\partial X} + V\frac{\partial \theta}{\partial Y} = \frac{1}{RePr}\left[\left(\frac{\partial^2\theta}{\partial X^2} + \frac{\partial^2\theta}{\partial Y^2}\right) - \frac{4\alpha}{\alpha+1}\frac{W}{\bar{W}}\right] \tag{12}$$

The solutions wanted for Eqs. (8–12) must satisfy the boundary conditions indicated with the aid of Fig. 2. As seen in this figure, the domain of interest (in the XY plane) is reduced to half a cross section, because of symmetry.

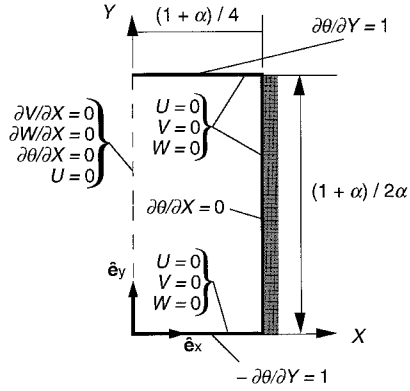

Fig. 2 Boundary conditions.

Mechanical Behavior

Most viscoelastic fluids show both viscosity dependence on shear rate and elastic behavior. To describe mathematically the mechanical behavior of this kind of fluid, relatively sophisticated constitutive models are needed. The generalized Newtonian liquid model, widely used for representing the viscosity dependence on shear rate, is not capable of predicting elastic mechanical behavior. In this work the Criminale–Ericksen–Filbey (CEF) equation is employed as constitutive equation.[22] It is similar to a second-order fluid, except that the coefficients are allowed to be functions of the rate of deformation. It is an attractive choice for this problem, because it is perhaps the simplest constitutive equation that can predict both shear thinning (or thickening) and nonzero normal stress differences in steady simple shear flows. The driving force that causes secondary flows in noncircular ducts is known to be related to the mechanism that generates second normal stress differences in steady simple shear flows (e.g., Townsend et al.[14]).

The CEF constitutive relation may be written as (Bird et al.[12])

$$\boldsymbol{\tau} = \eta(\dot{\gamma})\dot{\boldsymbol{\gamma}} - \tfrac{1}{2}\Psi_1(\dot{\gamma})\boldsymbol{\gamma}_{[2]} + \Psi_2(\dot{\gamma})\dot{\boldsymbol{\gamma}}^2 \tag{13}$$

The tensor $\boldsymbol{\gamma}_{[2]}$ is the convected derivative of the rate-of-deformation tensor, which is defined as (d/dt is the material time derivative):

$$\boldsymbol{\gamma}_{[2]} \equiv \frac{d\dot{\boldsymbol{\gamma}}}{dt} - [(\text{grad } \mathbf{v})^T\dot{\boldsymbol{\gamma}} + \dot{\boldsymbol{\gamma}}(\text{grad } \mathbf{v})] \tag{14}$$

The material functions that appear in the CEF relation [eq. (13)], namely, $\eta(\dot{\gamma})$, $\Psi_1(\dot{\gamma})$, and $\Psi_2(\dot{\gamma})$, should fit well experimental shear data for the flowing liquid. In this work the viscosity function employed is of the Carreau–Yasuda type (Bird et al.[12]):

$$\eta(\dot{\gamma}) = \eta_\infty + (\eta_0 - \eta_\infty)[1 + (\lambda\dot{\gamma})^a]^{(n-1)/a} \tag{15}$$

The stress coefficients $\Psi_1(\dot{\gamma})$ and $\Psi_2(\dot{\gamma})$ are assumed to be constant for simplicity. Preliminary tests, performed in the course of the present research, indicated that constant and variable normal stress coefficients yield the same qualitative results for typical dependencies of Ψ_1 and Ψ_2 on $\dot{\gamma}$.

In dimensionless form, Eq. (13) is written as

$$\boldsymbol{\tau}^* = (\eta^*/Re)\dot{\boldsymbol{\gamma}}^* - \tfrac{1}{2}\Psi_1^*\boldsymbol{\gamma}_{[2]}^* - \Psi_2^*\dot{\boldsymbol{\gamma}}^{*2} \tag{16}$$

where $\boldsymbol{\tau}^* \equiv \boldsymbol{\tau}/\rho\bar{w}^2$ and $\boldsymbol{\gamma}_{[2]}^* \equiv \boldsymbol{\gamma}_{[2]}/\dot{\gamma}_c^2$.

The dimensionless version of Eq. (15) is

$$\eta^* = \eta_\infty^* + (\eta_0^* - \eta_\infty^*)[1 + (We\,\dot{\gamma}^*)^a]^{(n-1)/a} \tag{17}$$

where

$$\eta_0^* \equiv \eta_0/\eta_c, \quad \eta_\infty^* \equiv \eta_\infty/\eta_c, \quad We \equiv \lambda\dot{\gamma}_c, \quad \dot{\gamma}^* \equiv \dot{\gamma}/\dot{\gamma}_c \tag{18}$$

Nusselt Numbers

Heat transfer at the bottom and top walls is represented by the corresponding Nusselt numbers:

$$Nu_b \equiv \frac{q_w D_h}{\kappa(\bar{T}_{w,b} - T_m)} = \frac{1}{\bar{\theta}_{w,b}}, \quad Nu_t \equiv \frac{q_w D_h}{\kappa(\bar{T}_{w,t} - T_m)} = \frac{1}{\bar{\theta}_{w,t}} \tag{19}$$

In the previous expressions, $\bar{T}_{w,b}$ and $\bar{T}_{w,t}$ are defined as

$$\bar{T}_{w,b} \equiv \frac{1}{B}\int_0^B T_{w,b}\,dx, \qquad \bar{T}_{w,t} \equiv \frac{1}{B}\int_0^B T_{w,t}\,dx \tag{20}$$

The quantities $\bar{\theta}_{w,b}$ and $\bar{\theta}_{w,t}$ are defined accordingly as

$$\bar{\theta}_{w,b} \equiv \frac{2}{\alpha+1}\int_0^{(\alpha+1)/2} \theta_{w,b}\,dX, \quad \bar{\theta}_{w,t} \equiv \frac{2}{\alpha+1}\int_0^{(\alpha+1)/2} \theta_{w,t}\,dX \tag{21}$$

Nu_m is defined as

$$Nu_m \equiv \frac{q_w D_h}{\kappa(\bar{T}_w - T_m)} = \frac{2Nu_b Nu_t}{Nu_t + Nu_b} \tag{22}$$

In the previous expression, the mean wall temperature is given by $\bar{T}_w \equiv (\bar{T}_{w,b} + \bar{T}_{w,t})/2$.

Numerical Solution

The previous system of differential equations was solved by means of the control-volume approach described by Patankar.[23] The coupling of momentum, continuity, energy, and constitutive equations was handled with the aid of the SIMPLE algorithm. The discretized algebraic system was solved through the line-by-line Thomas algorithm.

Difficulties in convergence were caused by the highly nonlinear character of the governing equations. To overcome these problems and obtain converged solutions, a zeroth-order continuation procedure in Ψ_2 and Ra was employed, starting from the solution for the Newtonian case with no natural convection.

The convergence was verified by observing the evolution of two different quantities, which should tend to zero as a converged solution is approached: 1) a normalized residual of the momentum equations in the vertical and transversal directions and 2) the global heat balance.

The mesh sizes employed were 22×42 for $\alpha = 1$, 22×22 for $\alpha = 2$, and 42×22 for $\alpha = 4$. These meshes have been chosen as a result of extensive mesh tests. For the cases that allowed comparisons with results available in literature, viz., no natural convection and Newtonian behavior, the agreement was within 0.5% both for $f.Re$ and Nu values. Details of the mesh tests are reported elsewhere.[21]

Results and Discussion

It is possible to analyze the present problem by means of two different approaches: 1) by investigating the effects of geometry and elasticity for a given fluid and 2) by investigating the effects of the different dimensionless parameters that appear in the above previous problem formulation.

The conclusions obtained with the first approach are directly applicable to engineering situations for the fluid under investigation, but it is generally not possible to draw conclusions for other fluids. Therefore, generality is lost. When this approach is adopted, the values of the parameters appearing in Eq. (15) are held fixed.

The second approach gives the relative importance of each dimensionless parameter. With this information, it is possible to make predictions for any fluid behaving according to the constitutive equation employed, as long as the values of the related dimensionless parameters are kept within the ranges investigated. However, varying one dimensionless parameter while maintaining all others fixed, generally means that a different fluid corresponds to each value of the varying parameter. For the flow of a given fluid, it may not be simple to extract engineering predictions from results presented in terms of dimensionless parameters. Therefore, the first approach is chosen in the present research, which is more suitable when comparisons with experimental results are desired.

The values of the parameters appearing in Eq. (15) are taken such as to fit the experimental data of a polyacrylamide solution employed in the experiments reported by Hartnett and Kostic.[6] These values are $\eta_0 = 0.282$ Pa s, $\eta_\infty = 3.85 \times 10^{-3}$ Pa s, $\lambda = 4.74$ s, $n = 0.494$, and $a = 0.942$.

Unfortunately, Hartnett and Kostic[6] seemingly did not characterize their polyacrylamide solution with respect to normal stress coefficients. For this reason, typical values for Ψ_1 and Ψ_2 were obtained in the literature. More specifically, the Ψ_1 results for a polyacrylamide solution found in p. 108 of Bird et al.[12] were employed to provide the order of magnitude of Ψ_1. To assess the influence of viscoelasticity, Ψ_1 was varied from zero to these values.

It is known that Ψ_2 for polymeric liquids are often in the range $-0.25\Psi_1 < \Psi_2 < -0.10\Psi_1$ (Bird et al.[12]). Thus, in the present research, the values of first- and second-normal stress coefficients are such that $\Psi_2 = -0.15\Psi_1$, for all cases investigated.

Figures 3a–3d, which pertrain to $\alpha = 1$, $Re = 1000$, and $Ra = 2 \times 10^6$, show some of the main features of the secondary flows and temperature distribution that occur in the xy plane. In Fig. 3a, no viscoelasticity is present, and therefore, the secondary flow is a result of natural convection only. It is seen in Fig. 3a that the flow is nearly stagnant close to the top wall. In the half bottom region, one large vortex is formed close to the vertical wall, while a small one appears adjacent to the symmetry plane. Accordingly, the isotherms are horizontal in the upper portion of the cross section, indicating pure conduction, and distorted by the convective effect of the vortices found in the half bottom region.

For a different thermal boundary condition, this four-vortex pattern was also observed by Nandakumar and co-workers[24] for this Ra range. Nandakumar et al.[24] also observed that in their case another solution displaying a two-vortex pattern is also possible in the range $91{,}000 < Ra < 165{,}000$ (i.e., a bifurcation). Similar dual solutions were obtained here and by Naccache[21] for smaller Rayleigh numbers and no viscoelasticity.

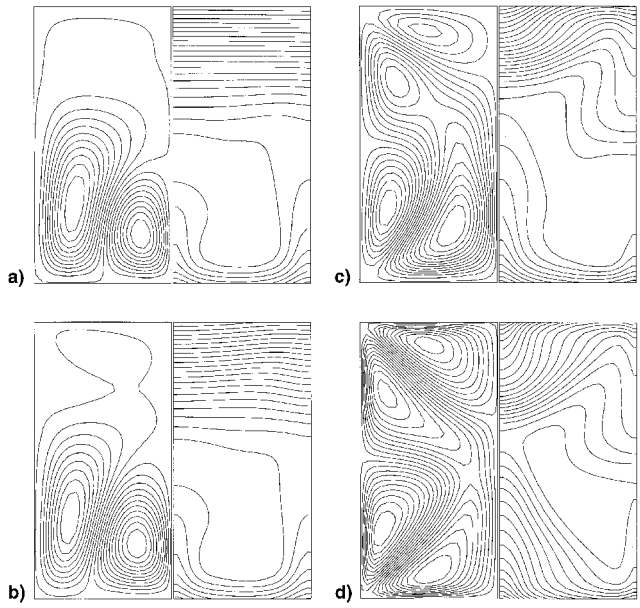

Fig. 3 Secondary flows

As Ψ_2^* is increased, some secondary flow activity starts developing at the upper portion of the cross section, as a consequence of the action of viscoelastic forces. Moreover, the symmetry plane vortices tend to grow, whereas the wall vortices tend to diminish. This onset of vortex activity at the upper portion of the test section clearly distorts in the isotherms. At $\Psi_2^* = 1 \times 10^{-5}$ (Fig. 3b), the symmetry plane vortices are larger than the wall vortices. At $\Psi_2^* = 1 \times 10^{-4}$ (Fig. 3c), two other vortices appear in the upper portion of the half cross section, which are weaker than the lower vortices. The upper vortices increase in size and intensity as Ψ_2^* is increased, so that at $\Psi_2^* = 1 \times 10^{-3}$ (Fig. 3d) the upper and lower flow patterns become about the same. Actually, at sufficiently high viscoelasticity, natural convection becomes negligible, and all four vortices become of equal size, intensity, and shape, symmetrically arranged in the half cross section.[7] Consequently, the isotherms also become symmetric with respect to the horizontal midplane.

The qualitative changes in flow pattern, illustrated in Fig. 3, have a strong impact in the heat transfer behavior. Firstly, it is interesting to note that Nu_t is either smaller or equal (in the limit of high Ψ_2^*) to Nu_b. Therefore, because Nu_m is a harmonic mean of the top- and bottom-wall Nusselt numbers, it has the same trends as Nu_t.

Figure 4 show the top (Fig. 4a) and bottom-wall (Fig. 4b) Nusselt numbers as functions of Ψ_2^*. When Ψ_2^* is small ($<10^{-7}$), natural convection prevails, and the Reynolds number has a rather small influence on the Nusselt numbers. This dependence on *Re* exists solely because of its influence on the wall shear rate, which affects the shear thinning viscosity. Heat transfer at the bottom wall is much more intense than at the top wall, where a nearly stratified situation occurs. At the other extreme where Ψ_2^* is large, viscoelasticity takes over buoyancy, and the Rayleigh number ceases to affect the Nusselt numbers. In fact, for large Ψ_2^*, the three Nusselt numbers become identical (i.e., $Nu_b = Nu_t = Nu_m$, as seen in Naccache and Souza Mendes[25]), because of the thermal symmetry that is approached in the limit of zero buoyancy force.

Viscoelasticity (through the second normal stress difference) causes the top-wall and mean Nusselt numbers to increase up to a certain value of Ψ_2^*, where the effect of the first normal stress difference (Ψ_1^*) becomes important,[25] as illustrated in Fig. 4a. This increase in Nu_t happens because of the new vortices that appear in the vicinity of the top wall as Ψ_2^* is increased.

Regarding the bottom-wall Nusselt number, viscoelasticity causes it to decrease up to a certain point, then increase up to a local maximum, and finally decrease again, as illustrated in Fig. 4b. This interesting trend is explained as follows, with the aid of the flow patterns shown in Fig. 3. In Fig. 3a it is seen that each of the two natural convection vortices interacts with roughly half of the bottom wall. The wall vortex is wider in the horizontal midplane region, and effectively exchanges heat with the cooler fluid in the midplane region. The symmetry–plane vortex is narrower in the horizontal midplane region, and cooling of its recirculating fluid is not as effective. Observing the shapes of the viscoelastic vortices shown in Fig. 3d, it is clear that the symmetry–plane vortex is the only one directly interacting with the bottom wall. This vortex, however, is nearly triangular in shape and has very little contact with the cooler fluid in the horizontal midplane region. This situation is obviously worse, as far as heat transfer is concerned, than the natural convection flow shown in Fig. 3a. Increasing Ψ_2^* further does not cause more changes in the vortex shapes, and the corresponding increase in the Nu_b curve is attributed to the increase of vortex intensity. The final decrease observed in the Nu_b curve is caused by the decrease in vortex intensity, which is caused by Ψ_1^* effects.[25]

The trends of the isotherms presented in Fig. 3 are in accordance with the *Nu* behavior shown in Fig. 4.

Note that the secondary flow velocities are about three orders of magnitude lower than the axial velocities. Nevertheless, the effect of these vortices on heat transfer is striking for the thermal boundary conditions investigated here. For other thermal boundary conditions, this might not be the case.

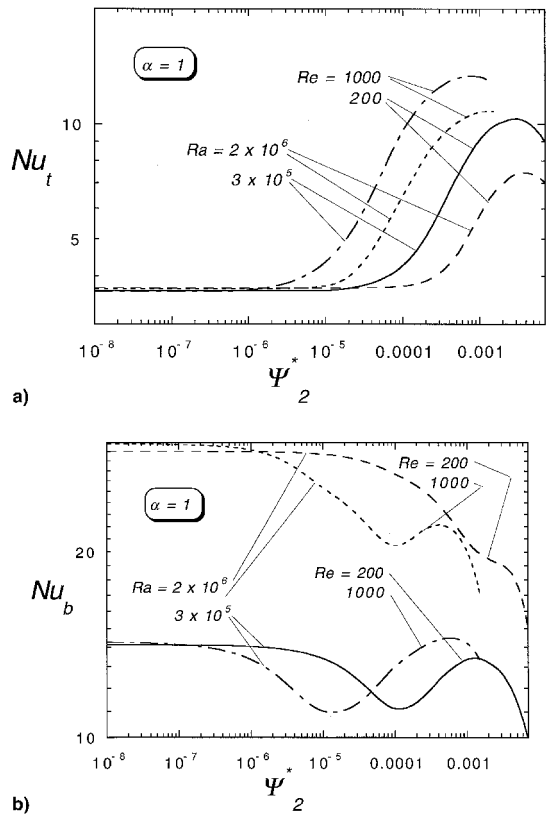

Fig. 4 *Nu* **vs** Ψ_2^***, for different** *Re* **and** *Ra* **(α = 1): a) mean and b) bottom-wall Nusselt numbers.**

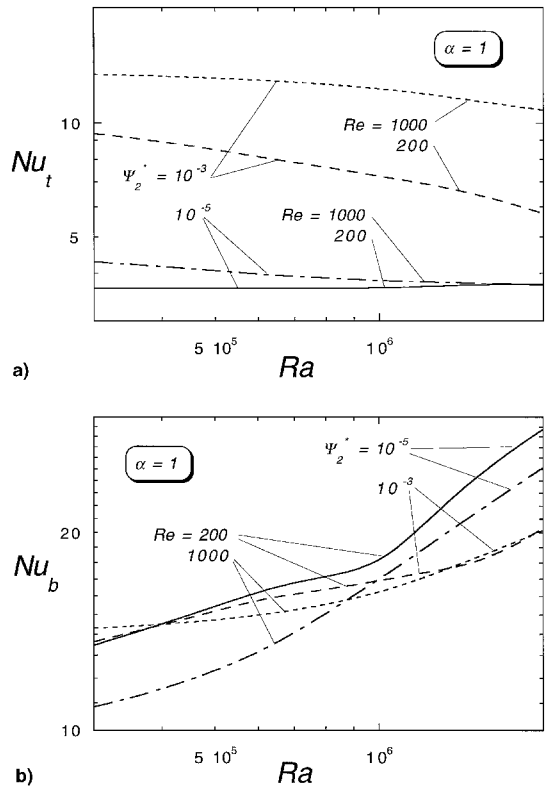

Fig. 5 *Nu* **vs** *Ra***: a) mean and b) bottom-wall Nusselt numbers.**

Figure 5a illustrates the dependence of Nu_t on Ra. For the high Ψ_2^* case ($\Psi_2^* = 10^{-3}$), the top-wall Nusselt number depends very mildly on Ra (Fig. 5a), indicating that, in this case, the viscoelastic force essentially governs the flow. For the lower Reynolds number case, namely, $Re = 200$, Nu_t tends to decrease faster in the high Ra range. Noting that the viscoelastic force is activated by the axial flow rate and increases with the Reynolds number, for $Re = 200$ the viscoelastic force is small and becomes comparable to the buoyancy force as Ra is increased. From the previous discussion on Fig. 4a, it is known that the top-wall Nusselt number for the viscoelasticity-dominated regime is larger than the one for the buoyancy-dominated regime. For the low Ψ_2^* case shown in Fig. 5a ($\Psi_2^* = 10^{-5}$), viscoelasticity is important in the low Ra range only, and the two Re curves become coincident for $Ra > 2 \times 10^6$, when buoyancy becomes dominant.

Figure 5b shows that Nu_b increases with Ra, as expected, and that the high Re, high Ψ_2^* cases are less sensitive to buoyancy effects than the low Re, low Ψ_2^* ones. These trends are predictable, and need no further discussion. It is worth mentioning, however, that while the curves for $Re = 1 \times 10^3$ indicate a smooth increase of Nu_b with Ra, the ones for $Re = 2 \times 10^2$ have rather abrupt increases in slope, at $Ra \simeq 10^6$ for $\Psi_2^* = 10^{-5}$, and at $Ra \simeq 1.5 \times 10^6$ for $\Psi_2^* = 10^{-3}$. This is a consequence of a secondary flow transition that occurs when buoyancy forces are dominant. This transition is characterized by the fact that two vortices are observed for low Ra, whereas four vortices occur at high values of Ra.

As illustrated in Fig. 6a, the dependence of the top-wall Nusselt number on Ψ_2^* is similar for the different aspect ratios investigated. However, the effects of both the first and the second normal stress differences are observed at higher Ψ_2^* as α is increased. When natural convection governs the secondary flows, Nu_t increases with α in the range investigated, because the natural-convection vortices start interacting with the top wall. However, this trend changes as Ψ_2^* is increased, because of the onset of viscoelastic effects.

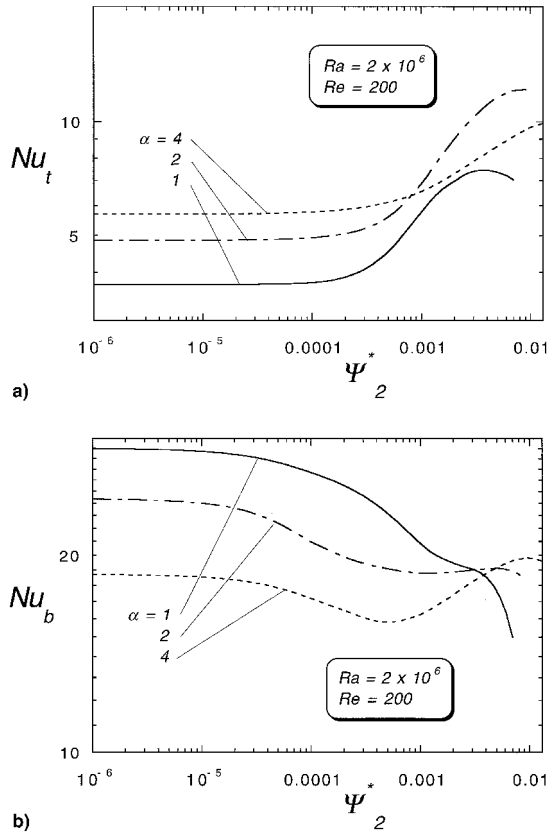

Fig. 6 *Nu* **vs** Ψ_2^***, for different** α **(***Re* **= 200 and** *Ra* **= 2 × 10⁶): a) mean and b) bottom-wall Nusselt numbers.**

Figure 6b shows that, for negligible viscoelasticity, the bottom-wall Nusselt number decreases as the aspect ratio is increased. This is a result of the weakening of the secondary flow, because of increased viscous resistance. For $\alpha = 1$, Nu_b decreases with Ψ_2^*, as explained earlier. For $\alpha = 2$ and 4 Nu_b changes little with Ψ_2^*.

Conclusions

Mixed convection in the fully developed flow of non-Newtonian fluids inside rectangular ducts has been investigated. The governing differential equations of mass, momentum, and energy were solved numerically by a finite volume technique. The viscoelastic behavior of the flowing fluid was described via the CEF constitutive equation.

Secondary flows are caused by buoyancy and by elastic forces related to the second normal stress difference. Other parameters influence secondary flows, such as the aspect ratio, the Reynolds number, and the first normal stress difference.

For a square duct ($\alpha = 1$) and no viscoelasticity, the flow is nearly stagnant close to the top wall. In the half bottom region, one large vortex is formed close to the vertical wall, while a small one appears adjacent to the symmetry plane. As viscoelasticity becomes important, vortex activity starts developing at the upper portion of the cross section, and the symmetry plane vortices tend to grow, while the wall vortices tend to diminish. Four other vortices appear in the upper portion of the cross section, which are initially weaker than the lower vortices, but increase in size and intensity as Ψ_2^* is increased. At sufficiently large Ψ_2^*, buoyancy becomes negligible, and symmetry with respect to the horizontal midplane is established in the flow.

As far as heat transfer is concerned, when Ψ_2^* is small natural convection prevails, and the Reynolds number influence on the Nusselt numbers is quite small. For $\alpha = 1$, heat transfer at the bottom wall is much more intense than at the top wall, where a nearly stratified situation occurs, and hence, buoyancy does not cause significant motion. For large Ψ_2^*, buoyancy forces become negligible, ceasing to affect heat transfer.

The mean Nusselt number for the viscoelasticity-dominated regime is larger than the one for the buoyancy-dominated regime. It increases up to a certain value of Ψ_2^*, where the effect of the first normal stress difference becomes important, which causes it to decrease. New vortices appear in the vicinity of the top wall when Ψ_2^* is increased, causing heat transfer enhancement. On the other hand, viscoelasticity causes the bottom-wall Nusselt number to decrease, because of a change in shape of the vortices adjacent to the bottom wall.

Because viscosity is typically a function of temperature, a study is under way to assess the impact of this effect on heat transfer for this flow.

Acknowledgments

This work was partially supported by the Ministério de Ciência e Tecnologia da Presidência da República—MCT/PR (Ministry of Science and Technology of the Brazilian Federal Government). The authors wish to express their gratitude to CNPq (Brazilian Council for the National Scientific and Technological Development) for the fellowships provided during the course of the present research.

References

[1]Hartnett, J. P., "Viscoelastic Fluids: A New Challenge in Heat Transfer," *Journal of Heat Transfer*, Vol. 114, No. 2, 1992, pp. 296–303.

[2]Mayné, G., "Secondary Flows of Non-Newtonian Fluids in Rectilinear Pipes," *Theoretical and Applied Rheology*, edited by P. Moldenaers and R. Keunings, Vol. 1, *Proceedings of the 11th International Congress on Rheology* (Brussels, Belgium), Elsevier, Amsterdam, 1992, pp. 146–148.

[3]Langlois, W. E., and Rivlin, R. S., "Slow Steady-State Flow of Viscoelastic Fluid Through Non-Circular Tubes," *Rendiconti di Ma-*

tematica, Series 5, Vol. 22, Nos. 1, 2, 1963, pp. 169–185.

[4]Oliver, D. R., "Non-Newtonian Heat Transfer: An Interesting Effect Observed in Non-Circular Tubes," *Transactions of the Institution of Chemical Engineers*, Vol. 47, No. 1, 1969, pp. 18–20.

[5]Mena, B., Best, G., Bautista, P., and Sanchez, T., "Heat Transfer in Non-Newtonian Flow Through Pipes," *Rheologica Acta*, Vol. 17, No. 4, 1978, pp. 454–457.

[6]Hartnett, J. P., and Kostic, M., "Heat Transfer to a Viscoelastic Fluid in Laminar Flow Through a Rectangular Channel," *International Journal of Heat and Mass Transfer*, Vol. 28, No. 6, 1985, pp. 1147–1155.

[7]Naccache, M. F., and Souza Mendes, P. R., "Heat Transfer in Non-Newtonian Flows Inside Rectangular Ducts," *Proceedings of the 4th Brazilian Thermal Science Meeting*, Brazilian Society of Mechanical Sciences, Rio de Janeiro, Brazil, 1992, pp. 573–576.

[8]Tachibana, M., Kawabata, N., and Genno, H., "Steady Laminar Flow of Power Law Fluids in the Inlet Region of Rectangular Ducts," *Journal of Rheology*, Vol. 30, No. 3, 1986, pp. 517–538.

[9]Lawal, A., and Mujumdar, A. S., "Laminar Flow and Heat Transfer in Power Law Fluids in Arbitrary Cross-Sectional Ducts," *Numerical Heat Transfer*, Vol. 8, No. 2, 1985, pp. 217–244.

[10]Lawal, A., "Mixed Convection Heat Transfer to Power Law Fluids in Arbitrary Cross-Sectional Ducts," *Journal of Heat Transfer*, Vol. 111, No. 2, 1989, pp. 399–406.

[11]Gringrich, W. K., Cho, Y. I., and Shyy, W., "Effects of Shear Thinning on Laminar Heat Transfer Behavior in Rectangular Duct," *International Journal of Heat and Mass Transfer*, Vol. 35, No. 11, 1992, pp. 2823–2836.

[12]Bird, R. B., Armstrong, R. C., and Hassager, O., "Dynamics of Polymeric Liquids," 2nd ed., Vol. 1, Wiley, New York, 1987.

[13]Winter, H. H., "Viscous Dissipation in Shear Flows of Molten Polymers," *Advances in Heat Transfer*, Vol. 13, 1977, pp. 205–267, Chap. 4.

[14]Townsend, P., Walters, K., and Waterhouse, W. M., "Secondary Flows in Pipes of Square Cross-Section and the Measurement of the Second Normal Stress Difference," *Journal of Non-Newtonian Fluid Mechanics*, Vol. 1, No. 2, 1976, pp. 107–123.

[15]Gervang, B., and Larsen, P. S., "Secondary Flows in Straight Ducts of Rectangular Cross Section," *Journal of Non-Newtonian Fluid Mechanics*, Vol. 39, No. 3, 1991, pp. 217–237.

[16]Chandrupatla, A. R., and Sastri, V. M. K., "Laminar Forced Convection Heat Transfer of a Non-Newtonian Fluid in a Square Duct," *International Journal of Heat and Mass Transfer*, Vol. 20, No. 12, 1977, pp. 1315–1324.

[17]Gao, S. X., and Hartnett, J. P., "Heat Transfer Behavior of Reiner-Rivlin Fluids in Rectangular Ducts," *International Journal of Heat and Mass Transfer*, Vol. 39, No. 6, 1996, pp. 1317–1324.

[18]Dunwoody, N. T., and Hamill, T. A., "Forced Convection in Lineal Flow of Non-Newtonian Fluids Through Rectangular Channels," *International Journal of Heat and Mass Transfer*, Vol. 23, No. 7, 1980, pp. 943–949.

[19]Kostic, M., "On Turbulent Drag and Heat Transfer Reduction Phenomena and Laminar Heat Transfer Enhancement in Non-Circular Duct Flow of Certain Non-Newtonian Fluids," *International Journal of Heat and Mass Transfer*, Vol. 37, Suppl. 1, March, 1994, pp. 133–147.

[20]Maughan, J. R., and Incropera, F. P., "Mixed Convection Heat Transfer with Longitudinal Fins in a Horizontal Parallel Plate Channel: Part I—Numerical Results," *Journal of Heat Transfer*, Vol. 112, No. 3, 1990, pp. 612–618.

[21]Naccache, M. F., "Mixed Convection in the Flow of Viscoelastic Fluids Through Rectangular Ducts," Ph.D. Dissertation, Dept. of Mechanical Engineering, Pontifí cia Universidade Católica, Rio de Janeiro, Brazil, 1993 (in Portuguese).

[22]Criminale, W. O., Ericksen, J. L., and Filbey, G. L., "Steady Shear Flow of Non-Newtonian Fluids," *Archives for Rational Mechanics and Analysis*, Vol. 1, No. 2, 1958, pp. 410–417.

[23]Patankar, S. V., "Numerical Heat Transfer and Fluid Flow," Hemisphere, New York, 1980.

[24]Nandakumar, K., Masliyah, J. H., and Law, H. S., "Bifurcation in Steady Laminar Mixed Convection Flow in Horizontal Ducts," *Journal of Fluid Mechanics*, Vol. 152, March, 1985, pp. 145–161.

[25]Naccache, M. F., and Souza Mendes, P. R., "Heat Transfer to Non-Newtonian Fluids in Laminar Flow Through Rectangular Ducts," *International Journal of Heat and Fluid Flow* (to be published).